An Effective Atlas-guided Brain image identification using X-rays

Dr. M Raja Sekar [1], Dr. N Sandhya [2]

[1]VNR Vignana Jyothi Institute of Engineering and Technology,
Professor Department Of Computer Science and Engineering,
Hyderabad, India
rajasekarm9@gmail.com

[2] VNR Vignana Jyothi Institute of Engineering and Technology,
Professor Department Of Computer Science and Engineering,
Hyderabad, India
sandhyanadela@gmail.com

Abstract: This paper explores using brain atlases for implicit identification of brain X-rays (BXRs). We developed a mechanism, which receives brain X-ray and build atlases. Developed system takes atlases as input and implicitly calculates the brain borders with formidable preciseness and capability. Apart from conventional atlas, we designed 2 two new atlases: (i) Implicitly calculated brain models by utilizing Magnetic resonance (MR) scans, and (ii) bi energy BXRs. We assess the designed system with each model on 34 BXRs from the BIRN Fmri and MRI dataset and another 34 BXRs from Alien Brain Atlas data set. We acquire an area under the **receiver-operating characteristic (ROC),** of about 96% for Alien Brain Atlas data set and 92% for BIRN Fmri and MRI datasets. Using the optimal operating point of the ROC curve, we acquired preciseness for segmentation of 87.91 ± 1.6% for alien Brain Atlas data set and 86.56 ± 2.9% for BIRN Fmri and MRI dataset. This procedure gives precise outcomes by using efficient procedures. The efficiency and reliability of designed procedure is also good.

Keywords: pixel-based brain image classifiers, BXRs, CXRs and feature assortment.

1. INTRODUCTION

Researchers have established the relation between brain abnormalities and various brain disorders such as Alcoholism [1-3], Schizophrenia [4-7], and Autism [8, 9]. The designed mechanism deduce the image and contour characteristics of brain areas from BXR images, and detects the disorders using pattern identification algorithms, computational learning algorithms and image processing techniques. Magnetic resonance (MR) scans of the brain are an important diagnostic procedure brain research. Developing and managing of MR image database incorporating segmentations is relatively easy process. Possible errors in Atlas-based brain identification using X-rays include type-I error and type-II error. Propagation capability of the query depends on availability of atlases databases.

Implicit brain detection is not only helpful for excellent texture synthesis, but also helpful for BXR screening in which brain boundaries are helpful to identify brain disorders or neurofibromatosis [10-11]. Brain boundaries also need to be detected precisely so that reconstruction of an exact 3D brain-bone model. Brain identification is difficult task due to (i) improper boundaries induced by covering structures of body parts, (ii) noise during acquisition of sample images, and (iii) anatomical shape changes caused by ill health and distortion of tissues. Brain edges contrast is usually very poor by means of the identical calculated intensity values at the boundaries of the brain and also surroundings of tissues. Apart from these difficulties, image presentation changes in between patients due to deviations in brain mineral deposits, body emotions and environmental factors, and posture of human brain during capture of an image using X-ray. Fig. 1 shows a typical brain
image structure variance across different persons, as well as fraudulent edges.

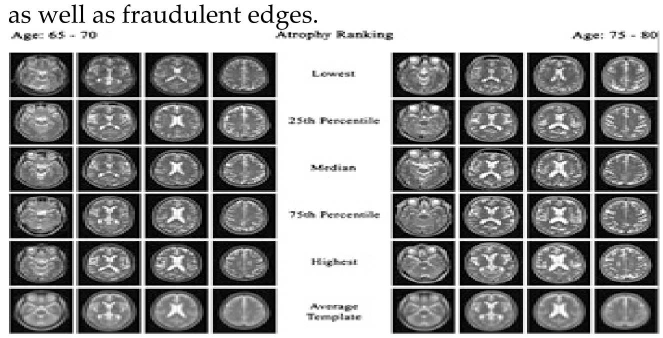

Fig.1 Area template image of human brain

It has been proved that prior-information algorithms are more efficient than no prior–

ISSN 2229-5518

information methods [12,13,3,14,15]. Prototype 'atlas' forms basis for prior based information method. In this paper, we carry out the research, which involves usage of atlas for implicit brain image deduction from BXRs. An example BXR image of the suggested method is exhibited in Fig. 2.

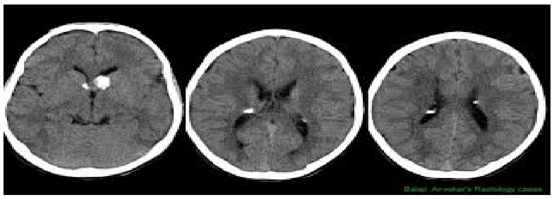

Fig. 2. Sample BXR images

In the context of this paper atlas can be defined as a collection of model X-ray pictures and their associated brain image boundaries. Three methods are used to construct image models: (i) X-ray image with explicitly traced brain image edges (Fig. 3); (ii) simulated X-ray and brain model image created from computed tomography (CT) scans images (Fig. 3); and (iii) BXRs generated from a scanner (Fig. 3). The atlases are constructed by using human brain X-ray images, generating a transformation for all pixels that permits the associating atlas brain mask to be transformed.

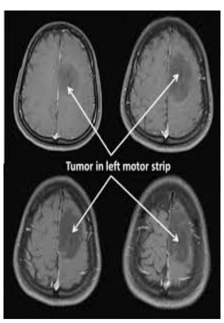

Fig. 3 Transformed pixels in brain image

We reviewed existing literature and our work in part 2. The databases utilized in our work are listed in Section 3.1. The methodology is described in section 3.2, which includes the atlas construction, model selection, and atlas registration. We provide the experimental results in section 4. Analysis and conclusions are included part 5.

2. LIITERATURE REVIEW

2.1. Atlas-based segmentation

There are several atlas databases available such as Allen Brain Atlas, BIRN fMRI and MRI data and Brain Cloud .In this paper we designed a frame work to solve the anomalies in multi-atlas segmentation. Two important methods which are used in this work are active models [16] and shape models [17]. Atlases is useful in medical image analysis especially in calculation of brain image [13,18,19] and heart image [12-19] edges. Multi-atlas method is more efficient compare to single atlas method [20-25] as it use many atlas models are used. Final segmentation can be formed by aggregation of all atlases, which are registered [21, 14, 22, 23, and 15]. The segmentation depends on nature of the atlases, which are registered.

2.2. Brain edge identification

Several methods are designed for implicit brain image identification. These methods based on edge detection a procedure, which is used to obtain the brain image pixels [25]. Brain image pixels are used to get complete brain image edges with the help of techniques like ellipses [28–30,7], parabolas [31] and Z transforms. Accuracy of geometric methods is more than that of edge detection algorithms as it detects brain image edges efficiently. Geometric methods are not appropriate for varying brain images and deformed brain images. Few researchers use geometric antiformable procedures to deal with the structural changes [25,11]. A modern approach for brain image identification is discussed in [10]. This method uses filter based orientation and multi-path method, which uses branch logic. This approach solves the huge variability in brain image structure. This method is not fully automatic method which needs initialization process.Edge gradients methods are more accurate than edge based methods in classifying brain and non-brain images [23]. Neighborhood shape methods are accurate in classifying pixels of brain image.

2.3. PROPOSED APPROACH

In this approach, brain atlases are used to identify patient brain images implicitly. In literature survey, we observed that no study is carried out on brain image identification. In our methodology, we used appropriate brain atlases, which consist of similar brain images. The average of all registered models constitutes brain image probability map for the brain image. Apart from manual portrait, we introduced two different approaches to construct the brain image atlases: models derived from BXR images and brain images acquired from a Philips dual energy CT scanner. The benefits of our proposed methodology :(i) the methodology implicitly identifies brain images by using scanners. (ii) The brain image atlases include the relation between the various parts of brain images. (iii) Apart from traditional methods, variations in brain structures can deal with registration method, which uses texture.

3. Methods

3.1. Data

Brain Cloud [24] which consists 447 BXRs, All BXRs have a size of 3000× 3000 pixels and a gray-scale color depth of 20 bits. The brain images are obtained with the help of digital image processing techniques [12-14]. The Brain Cloud is a freely available, biologist-friendly, stand-alone application for exploring the temporal dynamics and genetic control of transcription in the human prefrontal cortex across the lifespan. Brain Cloud was developed through collaboration between the Lieber Institute and NIMH [15]. In our experiment, we have used 35 reference models, which are manually made by an expert.

The Allen Mouse and Human Brain Atlases are projects within the Allen Institute for Brain Science, which seek to combine genomics with neuroma anatomy by creating gene expression plots for the mouse and human brain. This data set consists of 178 BXRs; 96 X-rays are related to normal patients and 78 X-rays are related to abnormal patients. All X-ray images are stored in 16 bit gray scale and of size 4000x4000. Brain imaging, magnetic resonance imaging of the head or skull, cranial magnetic resonance tomography (MRT), neurological MRI - they describe all the same radiological imaging technique for medical diagnostic. Magnetic resonance imaging of the human brain includes the anatomic description and the detection of lesions. Special techniques like diffusion weighted imaging; functional magnetic resonance imaging (fMRI) and spectroscopy provide also information about the function and chemical metabolites of the brain. MRI provides detailed pictures of brain and nerve tissues in multiple planes without obstruction by overlying bones. Brain MRI is the procedure of choice for most brain disorders. It provides clear images of the brainstem and posterior brain, which are difficult to view on a CT scan. It is also useful for the diagnosis of delineating disorders (disorders such as multiple sclerosis (MS) that cause destruction of the myelin sheath of the nerve).
With this noninvasive procedure also the estimation of blood stream and the flow of cerebrospinal fluid (CSF) are possible. Dissimilar MRA systems, also without contrast agents can display a vein or principal angiogram. MRI can separate tumors, inflammatory lesions, and other pathologies from the normal brain anatomy.
However, MRI scans are also used instead other methods to avoid the dangers of interventional procedures like angiography (DSA- digital subtraction angiography) as well as of repeated exposure to radiation as required for computed tomography (CT) and other X-ray examinations. The set contains both BXRs and Brain CTs of 220 patients. Brain radiographs were obtained with the help of KODAK-260 of 3900 × 3900 size.

3.2. Atlases

As brain image atlases, we used (i) classical BXRs and explicitly Identified brain image boundaries, (ii) brain image models constructed from computed tomography scan, and (iii) dual energy scanning CXR images.

3.2.1. Explicitly identified brain images

We have chosen 150 PA BXRs from the Brain Cloud and BIRN fMRI databases and identified the brain image edges using MATLAB Toolbox for the LabelMe Image database [39,40], which performs accurate online labeling capabilities. Explicitly identified brain image edges are shown in Fig. 3a. where posterior and interior parts of brain image is shown. In this illustration, the interior brain image boundary is shown in green while posterior

ISSN 2229-5518

brain image edge is shown in blue. The explicit boundaries are used in quantitative and qualitative analysis as reference standard.

3.2.2 X-rays and corresponding brain image models

Explicit identification is a difficult procedure for brain images, where most suitable BXRs can be obtained from explicit labels. We present a brain image atlases calculated from computed tomography scan. The brain image models are obtained by using computed tomography scan and BIRN fMRI dataset.

$ei(x_1;p)=\sum_{i=1}^{k}\sum p(\mu 0^{(i)} \mid xi)\log p(\mu o^{(i)} \mid \mu 1^{(i)})-$
$H(X_0 \mid x_1)^{\phi}(x_1)=\min_P(ei(x_1;P)/V_P$
(4)

Therefore, we project the maximum intensity of each column
in the axial plane to the coronal plane by
$dev(I^E_p \quad ,I^E_m) \quad =1/I^E_p \quad | \quad \min|x-x'|$
(5)
Where dev. is the greatest strength protrusion vector of image K_i; K_i is the k^{th} axial piece of CT MRI; $K_i[c_i]$ is the strength value of image K_i at i^{th} pole. We pretend the parallel X-ray image with the identical method by bulging the standard force at each column in the axial plane to the coronal plane by

$E(w) = \sum \min(||X_1(p) - X_2(p + w(p))||, t) + \sum (|Y(p)| + |Y(p)|) + \sum \min(|u(p) - u(q)|, d) + \min(|W(p) - W(q)|, d)$ (6)

Where E(w) is the average intensity projection vector of image I_k; I_k is the k^{th} slice of CT scan; and $I_k[ci]$ is the intensity value of image I_k at i^{th} pole.

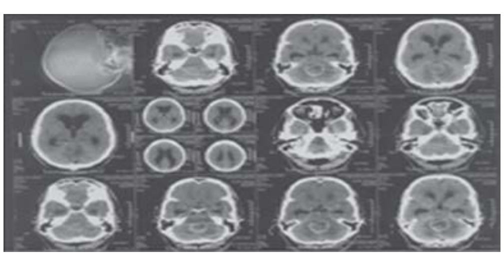

Fig.4 Illustration of brain images with deformations

We recap the bulge process for each axial slice, attaining the pretend X-ray and brain image standard in the coronal plane. In order to diminish the blare, we endeavor the strengths only privileged the thorax area. Fig. 4 illustrates the rib-bone building procedure from CT scans.

3.2.3. Dual energy CT

We expended dual energy scanners to attain brain images. Dual energy CT scans are a relatively new form of CT scanning that use separate X-ray energies to make images.The major adverse effects of a dual energy CT scan are related to the radiation exposure and the use of intravenous iodinated contrast (not always required). We used histogram equalization to enhance the contrast between brain and non-brain images (Fig. 3).

3.3. Selection of suitable Atlas

As registration is a tedious process, hence, we registered only a sample of atlas instead of registering population of atlases. We used brain image models to decrease shape difference between the patient's brain image and the atlas. We applied cross-bilateral filtering to reduce the noise in the image pixels but preserve the important edges. After filtering, we used the sober edge identification procedure [43] to acquire the edge map brain image. Fig. 5 displays the edge detection results on filtered X-rays. We measure the similarity of the edge maps of X-ray images using the equation

$MIN_{I2} = \langle \max(Ik[ci]) \rangle, \quad \forall C_i \in Ik, i = 1, 2, \ldots, C,$
$|IE$ (7)

The scheme calculates the vastness MIN concerning the edge map of the forbearing X-ray and the threshold plan of every X-ray in the atlas, and retrieves the most similar top-n brain atlas prototypes.

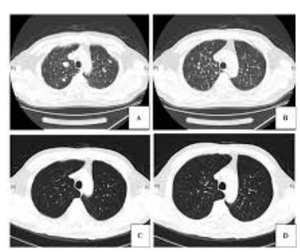

Fig. 5 Patient-Specific brain images

After generating the subsection, we showed the chosen X-rays to the patient's X-ray to shape a patient-specific rib-bone standard.

3.4 Atlas Cataloguing

Brain image standard is composed with the assistance of brain image recording process. We expended progressive non-rigid recording process that resolves greatest of the difficulties in recording procedure itself. The process computes plotting pixels between an individual X-ray and model. Brain images and constructed brain image models are aligned with mapping technique. Advanced Scale Invariant Feature Transform is useful for estimated values of local regions. Histogram equalization is used in the extraction of images.

$$E(v)=£ \quad X_{(i)} | Y_{(j)}-\{W_{(i)} | V_{(i)}\}-\mu^1-\mu^2[x_i-y_i] \quad (7)$$

There are 12 couples of ribs in a normal human rib cage. Though the precise number depends on respiration, typically, six to nine rib pairs are visible in the lung area. The rib bones below the diaphragm are hardly visible in a CXR because of the abdomen shadow. Therefore, we define the lung area as the search area for ribs. To detect the lung area, we used a lung segmentation algorithm.

In 4.2 sections, we analyze the correctness of suggested method with assessments of brain image probability maps. Edge maps of brain mages are used for quantitative and qualitative analysis of proposed system. Probability map of brain images is calculated by the average of registered models.

Fig 6. Probability map of brain image

Fig. 6 displays an instance of calculated probability map of brain images. In this paper we discusses three types of atlas models namely: (i) Manually marked edge brain images and

usual X-rays (ii) Brain image models and computer-generated X-rays are calculated from CT scans and (iii) Images computed from dual energy scanners

We verified the proposed method complexity with every model.

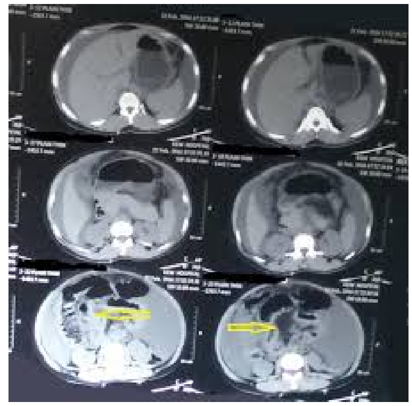

Fig. 7 Calculated probabilities of atlas models

Fig. 7 displays calculated probabilities with all atlas models for the same brain images. As shown in common characteristics figures, the proposed procedure allocates greater probabilities to brain image areas than non-brain image areas. The pictorial outcomes also display that the procedure yields comparatively less precise edges at the lowest portion of the brain. This is happened, as there is a pixel intensity differences in between brain image and non-brain image.

3.5 Projected Algorithm

Step1: Gather the training brain images
Step2: Discover the bin standards of each brain image ($G[X_b][Y_b][n_f]$)
Step3: Construct Face prototype ($TF[X_b][Y_b]$)
Step4: Compute different faces (FD=G-GT)
Step5: Ruminate analysis brain image.
Step6: Locate FT.
Step7: Evaluate DTF=FT-TF
Step8: Estimate HTDF=FTD-FD
Step9: If the summary of the alterations of the values designed in step7 is less than the maximum value then the image is matched and displayed

$$H(x, x) = (x^t x + 1)^d \quad (8)$$

$$H(x, x) = x^t x \quad (9)$$

$K_{int}(A,B)=A.B$ (10)

$Mi(t)=wtif(x) + wibi$ (11)

$M(t) = w^T g(t) + c$ (12)

$D_{ij}(x)=w^t_{ij}f(x) + b_{ij}$ (13)

$R_i=\{x/D_{ij}>0, j=1, 2, 3, \ldots\ldots\ldots n, i\neq j$ (14)

3.6 Initialization of Brain Images

With the help of training images, construct a brain image matrix. Each brain image is characterized as a brain image matrix. Each brain image is presented by a vector of size = h*w and placed as a row vector.

1. Calculate the brain image mean face
2. Normalizing the training brain images by subtracting average brain matrix from brain matrix.
3. Determine Covariance matrix.
4. Compute characteristic vector and characteristic values.
5. Arrange characteristic vectors to get utmost meaningful ones.
6. Estimate brain image Space.
7. Calculate weights of training image

The Eigen face process has difficulties in identifying faces in different illuminations and adjustments. In the case of Eigen brain images we requisite frontal edges. There are six main chunks and task of each block is given below.

1. The achievement function.
This is the starting point of brain image authentication method. In this component brain image is assumed as in put to the block graph. In this segment, brain image of the individual will be obtained. This function obtain brain image of individual in distinctive situations.
2. Preprocessing module: To improve the identification ability of the procedure, brain images are regulated.

Following are the preprocessing phases

(i) Standardization of brain image: It is helpful to alteration the obtained brain image magnitude. Generally brain recognition Schemes operates on brain image of size 80×80
(ii) Histogram equalization: This technique is helpful for matching too dark or too sunny brain images. It is moreover beneficial to improve the excellence of brain image, which leads to the improvement of face recognition Scheme.
(iii) Mean Sifting: Mean Sifting is beneficial for cleaning the deafening brain images. Improvement of median filtering is it wipes brain images without loosing data.
(iv) High –Pass filtering: This filter is useful for extracting features from image based on facial outlines. To obtain the image details such as contours and detecting edges this image filter is useful.
(v) Contextual elimination: To compact with brain data itself, contextual of brain image noise must be removed. This is very important for brain identification scheme in the case of entire information of brain is expended
(vi) Preprocessing component must need competence of outcome of brain outline.

The values of probability maps are used to find different operating points on the receiver operating characteristic curve. With a great threshold, great intensity values are categorized as brain, yielding less sensitivity and great specificity. Threshold and intensity values are used for brain image classification. Proposed models specificity and sensitivity can also calculated from proposed algorithm. As a result of proposed method, increase its sensitivity but reduce the specificity. Fig. 8 displays the ROC curves obtained for different datasets.

The performance of BIRN Fmri dataset is more compare to performance of Fmri dataset, overall performance of BIRN Fmri dataset is around 96% and where as performance of Fmri dataset is around 92% area under receiver operating characteristic curve. Blue curves represent BIRN Fmri dataset and red cred curves represent Fmri dataset. There are two stages in collecting the BIRN Fmri dataset namely: (i) Images are captured using analog systems (ii) In this stage images are transformed into digital format. Consequently, the images have a uniform pixel intensity values. However, digital scanners obtained the X-rays.

Dataset	Image set1			Image set2		
	Precision	FAR	FRR	Precision	FAR	FRR
BIRN Fmri	.7310	.3512	.0401	.7370	.2502	.0403
Frmi	.8820	.1002	.0412	.7624	.3004	.3111
BrainWeb	.8201	.1001	.0101	.7231	.3511	.1110

Table 1. Comparison of Database

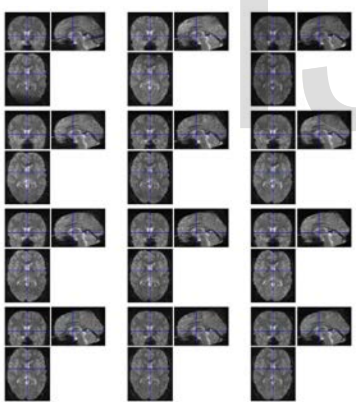

Fig.8 BIRN Fmri brain image data set

$$P(x) = \left[\frac{\exp(-\frac{1}{2}\sum \frac{p_i^{\,2}}{\blacklozenge_i})}{(2\ )^{m/2} \sum_{i=1}^{m} \blacklozenge_i^{\,1/2}} \right] \left[\frac{\exp(-\frac{\in^2(x)}{2\rho})}{(2\pi\rho)^{1/2}} \right] \quad (15)$$

The quality of images acquired by digital scanners has much higher than the images captured by analog systems.

4. EXPERIMENTATIONS

4.1. Assessment approach

One crucial test for brain image methods is to obtain a locus to validate the system functioning and relate various methods. Commonly, some specialists are requested to outline the boundaries, preferably several times. Then, the collection of expert markings are combined into one reference standard either taking the average of markings or using a more refined procedure such as PLE (Performance Level Estimation).

$$w_i^t f(x) + b_i > w_j^t f(x) + b_j \text{ for } i \neq j,\ j=1\ldots..n \quad (16)$$

Though, expert outlining is a tiresome procedure, specifically for brain image boundaries considering that BXRs essential at least 22 manual labels (for noticeable brain images). Hence, presently available brain image algorithms suffer from a dearth of benchmarks and such methods have been examined on restricted datasets. For illustration, the procedure in is examined only on 12 BXRs. In investigators explicitly outlined the brain image edges of 30 X-rays, and assessed their procedure on this data set. One of the major problems in existing methods is lack of reference edges in brain images.

4.2 Stimulating X-rays

Brain image segmentation is interesting due to brain image dissimilarities between the individuals. Brain image bone mineral density, respiration, body movement during X-ray captures and disease in the lung region affects the rib-bone shape and number of visible ribs. Fig. 9 shows the functioning of our system in this challenging situation. The scheme is able to locate the ribs given satisfactory texture report for the rib region. We register the rib models to the patient X-ray using a non-rigid registration approach. Therefore, our system successfully addresses the rib-shape variance between patients.

However, it cannot detect the ribs when the intensity difference between brain region and intercostals areas is poor.

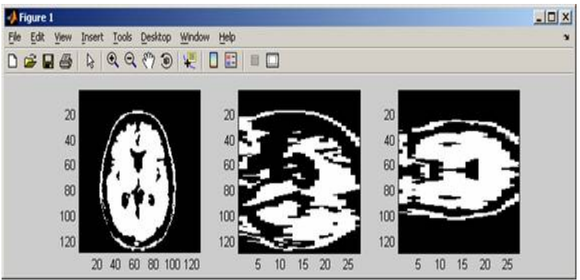

Fig. 9 Simulation of brain images by using MATLAB

5. CONCLUSIONS

Here we suggest an atlas-based method to obtain the brain image edge on classical BXRs. Given an individual X-ray, the method first selects the greatest related models in the atlas set and then registers them to an individual X-ray. So atlas prototypes, in addition to operating manually defined prototypes, we suggest two complementary atlases: (i) computer-generated prototypes processed from CT scan, and (ii) brain images from dual energy scanners. During the registration method, we handle the change mapping between the individual X-ray and model X-ray by processing the area resemblances between the X-rays. Then, we employ the subsequent change to the model brain image masks. The average of all registered models creates the rib bone probability map for the patient X-ray.

The suggested scheme constructs the individual brain model as a probability function in which each pixel intensity indicates the pixel's probability of being part of the brain image structure. In order to measure the functioning of the procedure, we calculated the ROC curves founded on the calculated likelihood maps. We succeeded an AUC of nearly 96% for the BIRN Fmri dataset and 94% for the MRI dataset. To calculate the brain image borders, we fixed the threshold for the probability map with the threshold set by the ideal point on the ROC curve. We attained 88% accuracy, 77% sensitivity, and 94% specificity on a public BXR set.

The probability atlases and edge results exhibited that the scheme fruitfully traces the brain images if there is acceptable texture report. It fruitfully reports the brain profile difference between

abase	Modified brain Images			Non-modified brain Images		
	Precision	FAR	FRR	Precision	FAR	FRR
Imageset3						
BWeb	.6211	.3881	.1100	.6511	.38811	.1100
BCloud	.7221	.1999	.1888	.6999	.1888	.1888
BData	.7911	.1122	.2822	.7911	.1100	.2900
BMap	.8513	.1110	.1101	.8512	.1011	.1101
Imageset4						
BWeb	.7120	.1110	.1010	1.0011	.0010	.0111
BCloud	.8011	0.1101	0.1100	0.8011	0.2000	.0111
BData	.3911	.0110	.8810	.4909	.1111	.9811
BMap	.8811	.1111	.0112	.8807	.8111	.0111
Imageset5						
BWeb	.6700	.7700	.1901	.6011	1.0111	.1009
BCloud	.7511	.1000	.1770	.7221	.1111	.1010
BData	.3881	.8811	.1111	.4884	.8811	.0101
BMap	.8220	.0220	.1110	.8110	.1111	.1188
Imageset 6						
BWeb	.3441	.8890	.8981	.4771	.0888	.8880
BCloud	.6001	.5810	.0110	.6880	.5881	.0011
BData	.3885	.1111	.8777	.3998	.1111	.8889
BMap	1.010	.0101	.1011	.8810	.0111	.0111
Imageset 7						
BWeb	.8889	.1911	.0111	.6688	.5811	.1100
BCloud	.9119	.8888	.1100	.5880	.1101	.1101
BData	0.4227	.8645	.0101	.4077	.1199	.1111
BMap	.8779	.1101	.0111	.8888	.1101	.1001
Imageset 8						
BWeb	.7860	.1101	.1210	.7811	.1101	.1811
BCloud	.0110	.1101	.1101	.7791	.1810	.0100
BData	.4651	.1011	.8891	.4567	.1101	.8887
BMap	.8888	.0111	.0101	.8401	.1101	.1001
Imageset 9						
BWeb	.4543	.1101	.8857	.4122	.1100	.8673
BCloud	.7121	.1811	.1110	.9810	.0100	.1781
BData	.5411	.1110	.8777	.3411	.0001	.8879
BMap	.6340	.1911	.1111	.8211	.1111	.1000
Imageset 10						
BWeb	.5400	.1101	.8100	.3411	.1100	1.0011
BCloud	.8781	.3881	.1111	.6811	.4611	.0011
BData	.3810	.0101	.8899	.4911	.1101	1.0011
BMap	.8300	.1101	.1101	.6741	.1010	.6501

Table2. Comparison of different brain datasets

individuals and the number of perceptible brain image due to individual pose deviations. The procedure yields comparatively less precise edges at the lowermost part of the brain. This is due to the feeble intensity dissimilarity between the brain image and boundaries. The frontal brain image is not as noticeably observable as subsequent brain on X-ray images. Hence, our appearance-based style might not find the frontal brain image as precisely as the subsequent brain image. We related our outcomes with the procedures in the literature by examining the procedure on a public dataset. Our complete system functioning is comparable with the modern approach and familiar to individual viewer enactment.

6. REFERENCES

1. S. Jaeger, A.Karargyris, S. Antani, and G. Thomas , "Detecting tube –culosis in radiographs using combined lung masks", Proc. Int. IEEE Eng. Med. Biol. Soc., vol.34 pp. 89- 99, 2014.
2. G. Coppini, M. Miniati, S. Monti, M. Paterni,R.Favilla, and E.M. Fer- deghini, " A computer- aided diagnosis approach for emphysema recognition in chest radiography", Med. Eng.Phy., vol. 35, pp. 63-73, 2013.
3. S. Candermir, S.Jaeger, K. Palaniappan, S. Antani, and G.Thoma, "Graph-cut based automatic lung boundary detection in chest radio-graphs," in IEEE Healthcare Technol. Conf: Translat. Eng. Health Med., 2015, pp. 31- 34, 2014.
4. B. Ginneken, M. Stegmann and M. Loog, "Segmentation of anatomical structures in chest radiographs using supervised methods: A comparative study on public database, "Med. Image Anal., vol. 10, pp. 19-4, 2015.
5. J. Lotjonen, R. Wolz, J. Koikkalainen, L.Thurfjell, G. Waldemar, H. Soininen, and D.Rueckert, " Fast and robust multi atlas segmentation of brain magnetic resonance images" NeuroImage, vol 15,pp. 45-59, 2014.
6. T. Kim, K. Lee, and S. Lee., " Generative image Segmentation using random walks with restart", Human brain mapping , vol 16, pp .78-89, 2014.
7. M. Morel and G. Yu. Asift., "A new framework for fully affine invariant image comparison" SIAM Journal on Imaging Sciences, vol 27, pp.79-85, 2015.
8. H. Bay, T. Tuytelaars, and L. V. Gool. , "Evaluation of atlas selection strategies for atlas based image segmentation with application", Med. Imaging, pp. 34-45, 2013.
9. Ruecckert, Sonoda and Hayes, "Non rigid registration using free form deformation",Application to breast MR images,vol. 45, pp.89-92, 2014.
10. Sederberg and T.W. Parry,"Free form deformation and solid geometric models", Computer Graphics, vol. 23, pp.452-465, 2013.
11. Rohlfing and Maurer, "Evaluation of atlas selection strategies for atlas-based image segmentation with application to confocal microscopic images of bee brains", Med Imag, vol.23, pp.56-76, 2014.
12. D. Cool, D. Chillet and J. Guyon, "Tissue based affine registration of brain images to form a vascular density atlas", Lecture Notes in Computer Science, pp.234-245, 2014.
13. N. Passat, C. Ronse and Baruthio, "Cerebral vascular atlas generation for anatomical knowledge modeling and segmentation purpose", Computer Vision and Pattern Recognition, vol. 69, pp. 934-52, 2015.
14. N. E. Manghat, G. J. Morgan and Hughes," Multi detector row computed tomography: imaging the coronary arteries",Clinical radiology, vol. 60, pp. 939-54, 2013.
15. P. M. A. van Ooijen, K. Y. Ho and Dorgelo, "Coronary Artery Imaging with Multidetector CT: Visualization Issues", Radiographics, vol.24, no pp.345-67, 2015.

16. C. Kirbas and F. Quek , "Vessel extraction techniques and algorithms: a survey", Bioinformatics and Bioengineering", vol. 34, no pp345-65, 2015.

17. S. Aylward and E. Built,"Initialization, noise, singularities, and scale in height ridge traversal for tubular objec centerline extraction", in Medical I maging, vol. 21, no pp. 34-36, 2013.

18. W. R. Crum and D.L. G. Hill ,"Information theoretic similarity measures in rigid registration", The EM Algorithm and Extension, vol. 45, pp.45-65, 2014.

19. B.M. Dawant et al., " Brain Atlas Deformation in the presence of Large Space occupying Tumors", MICCAI vol. 34, pp.456-76, 2015.

20. M. Bach Cuadra et al., "Atlas based Segmentation of Pathological Brains using a Model of Tumor Growth", MIC-CIA, vol. 56, pp 456-64, 2015.

21. J.P. Thirion, "Fast non rigid matching of 3D Medical Images", SPIE Med Img, vol.45, pp. 438-456, 2015.

22. Anjari M, Srinivasan and Hajnal JV," Diffusion tensor imaging with tract-based spatial statistics reveals localwhite matter abnormalities in preterm infants", SPIE Med Img vol.49, pp.345-78, 2013.

23. Collignon A, Males,"Automated multimodality medical image registration using information theory", Computational Imaging and Vision, vol. 56, pp.345-78, 2013.

24. Dubois J and Perrin M," A feasibility study using quantitative diffusion tensor imaging and tractography" in NeuroImage, vol.34, pp.345-67, 2012.

25. Glass HC, Bonifacio SL and Shimotake T," Neurology current treatment options in Neurology,vol. 35, pp. 32- 45, 2015.